Development ePress. Posted online 19 March 2015
 | Development (2015) 142, 1-11 doi:10.1242/dev.119479

RESEARCH ARTICLE

The *C. elegans* COE transcription factor UNC-3 activates lineage-specific apoptosis and affects neurite growth in the RID lineage

Jinbo Wang[1,2], Jyothsna Chitturi[3], Qinglan Ge[1,2], Valeriya Laskova[3], Wei Wang[1], Xia Li[1], Mei Ding[1], Mei Zhen[3,*] and Xun Huang[1,*]

ABSTRACT

Mechanisms that regulate apoptosis in a temporal and lineage-specific manner remain poorly understood. The COE (Collier/Olf/EBF) transcription factors have been implicated in the development of many cell types, including neurons. Here, we show that the sole *Caenorhabditis elegans* COE protein, UNC-3, together with a histone acetyltransferase, CBP-1/P300, specifies lineage-specific apoptosis and certain aspects of neurite trajectory. During embryogenesis, the RID progenitor cell gives rise to the RID neuron and RID sister cell; the latter undergoes apoptosis shortly after cell division upon expression of the pro-apoptotic gene *egl-1*. We observe UNC-3 expression in the RID progenitor, and the absence of UNC-3 results in the failure of the RID lineage to express a P*egl-1*::GFP reporter and in the survival of the RID sister cell. Lastly, UNC-3 interacts with CBP-1, and *cbp-1* mutants exhibit a similar RID phenotype to *unc-3*. Thus, in addition to playing a role in neuronal terminal differentiation, UNC-3 is a cell lineage-specific regulator of apoptosis.

KEY WORDS: UNC-3, Apoptosis, EGL-1, RID neuron, *C. elegans*

INTRODUCTION

Apoptosis plays crucial roles in development. During both embryogenesis and postnatal development many neurons and glial cells are eliminated through programmed cell death. An inappropriate level of cell death, either too low or too high, has been associated with congenital nervous system anomalies, autonomic disorders and neurodegenerative diseases (Oppenheim, 1991). Studies in *C. elegans* have contributed significantly to our understanding of the molecular pathways that execute programmed cell death (Ellis et al., 1991; Horvitz et al., 1994; Denning et al., 2013). Owing to a largely invariant cell lineage and the fact that a majority of apoptotic events occur shortly after the final round of cell division during *C. elegans* development, apoptotic events are readily observed and quantifiable (Kimble and Hirsh, 1979; Sulston et al., 1983). Genetic screens have been carried out to isolate mutants that either fail to execute apoptosis or exhibit excessive apoptosis (Sulston and Horvitz, 1981; Ellis and Horvitz, 1986). These mutants led to the identification of components of the core cell death pathway, including the apoptotic activator EGL-1 (Conradt and Horvitz, 1998), the anti-apoptotic factor CED-9 (Hengartner et al., 1992), the caspase activator CED-4 (Yuan and Horvitz, 1992) and the pro-caspase CED-3 (Ellis and Horvitz, 1986). These cell death executors are conserved in many metazoans (Danial and Korsmeyer, 2004).

A fundamental question remains as to how animals achieve cell type-specific and temporal regulation of apoptosis. Current studies suggest that regulatory pathways triggered by developmental (or damage) signals converge on the activation of the core cell death machinery to specify the fate of particular cells (Conradt, 2009). For example, in the hermaphrodite, TRA-1 (a global transcriptional regulator of somatic sexual fate) inhibits *egl-1* expression in the hermaphrodite-specific neurons (HSNs) (Conradt and Horvitz, 1999), but promotes *egl-1* expression in the male-specific cephalic companion neurons (CEMs) through inhibiting the transcription factor CEH-30 (Nehme et al., 2010). Asymmetrically distributed in the neurosecretory motor neuron (NSM) and its sister cell, the C2H2 zinc finger transcription factor CES-1 blocks the expression of *egl-1* in the NSM cell by competing against the basic helix-loop-helix (bHLH) transcription factors HLH-2 and HLH-3, which activate *egl-1* expression (Hatzold and Conradt, 2008). Diverse lineage-specific regulators of apoptosis have also been identified in other cells: the caudal-type homeodomain transcription factor PAL-1 promotes the death of the tail-spike cell by activating *ced-3* expression (Maurer et al., 2007); CEH-34 (Six family homeodomain protein) and EYA-1 (Eyes absent ortholog) promote the death of the sister cell of the M4 pharyngeal neuron (Hirose et al., 2010); the Hox proteins, including MAB-5 (Liu et al., 2006) and LIN-39 (Potts et al., 2009), are involved in programmed cell death in the P blast lineage that gives rise to postembryonic motor neurons.

The COE (Collier/Olf/EBF) family transcription factors share a DNA-binding domain that contains an atypical zinc finger domain, an IPT (immunoglobulin-like/plexin/transcription factor) domain that mediates both DNA and protein interactions, an HLH dimerization domain, and an unstructured C-terminal transcription-activation region (Hagman et al., 1995). COE family transcription factors include EBF1-4 in mammals, EBF2 and EBF3 in *Xenopus*, Ebf2 (Zcoe2) in zebrafish, Knot (Collier) in *Drosophila* and UNC-3 in *C. elegans* (Liberg et al., 2002). COE proteins function in the differentiation and specification of neurons (Garel et al., 1999), B lymphocytes (Lin and Grosschedl, 1995), adipocytes (Akerblad et al., 2002), osteoclasts (Kieslinger et al., 2005) and muscles (Crozatier and Vincent, 1999).

C. elegans UNC-3 plays diverse, lineage-specific roles in neuronal fate specification. UNC-3 is required for the postmitotic hindgut hypodermal Y cell to redifferentiate into a PDA motor neuron (Richard et al., 2011; Zuryn et al., 2014). UNC-3 promotes the identity of the ASI chemosensory neuron by activating the expression of ASI-specific genes and repressing alternative neuronal programs (Kim et al., 2005). In a fraction of cholinergic motor neurons, UNC-3 functions as the terminal selector for cholinergic fate (Kratsios et al., 2012) and further restricts the

[1]State Key Laboratory of Molecular and Developmental Biology, Institute of Genetics and Developmental Biology, Chinese Academy of Sciences, Beijing 100101, China. [2]University of Chinese Academy of Sciences, Beijing 100049, China. [3]Lunenfeld and Tanebaum Research Institute, University of Toronto, Toronto, Ontario, Canada M5G 1X5.

*Authors for correspondence (xhuang@genetics.ac.cn; zhen@lunenfeld.ca)

Received 5 November 2014; Accepted 17 February 2015

Development (2015) 142, 1-11 doi:10.1242/dev.119479

identity of the VA and VB subclass cholinergic motor neurons by repressing the VC-type subclass fate (Prasad et al., 2008). Loss of *unc-3* also leads to modest axon defasciculation and pathfinding defects (Wightman et al., 1997; Prasad et al., 1998).

Here we report a previously unknown function of UNC-3 in regulating apoptosis and neurite growth in specific neuronal lineages. In *unc-3* mutants, P*egl-1*::GFP reporter expression was lost in the RID lineage associated with the survival of the RID sister cell, which undergoes apoptosis in wild-type animals. Moreover, UNC-3 interacts with histone acetyltransferase CBP-1/P300, and *cbp-1* mutants exhibit the same RID phenotype as *unc-3*. Our results indicate that UNC-3, together with CBP-1, regulates a lineage-specific apoptosis event that ensures the specification of a single RID neuron.

RESULTS

UNC-3 affects the development of the RID cell lineage

The *C. elegans* nervous system consists of 302 neurons of 118 subtypes, each with distinct morphology, connectivity and position. One class, consisting of a single neuron, RID, is born during embryogenesis. The RID soma, which resides in the anterior dorsal ganglion, extends a single process that initially grows ventrally to join the ventral nerve cord, then loops back to the dorsal cord, followed by a posterior outgrowth along the dorsal nerve cord (Fig. 1B). The unipolar neurite of RID is functionally compartmentalized: the ventral/dorsal loop receives synaptic inputs from the ALA, AVB and PVC interneurons, and hence functions as a dendritic region; the anterior-posterior outgrowth resembles an axonal region, making synaptic outputs to hypodermis, muscles and other motor neurons (White et al., 1986).

To identify genes that regulate RID development, we performed a genetic screen using the fluorescent marker *hpIs162* [P*ceh-10*::wCherry], which is expressed strongly in the RID, AIY, CAN neurons, an unidentified support cell, and weakly in the ALA neuron. We isolated two loss-of-function alleles of *unc-3* that change the reporter expression pattern: *xd86* (R176 to opal stop) and *xd106* (W280 to opal stop) (Fig. 1A). In both alleles, ~70% of animals harbor a pair of P*ceh-10*::wCherry-positive neurons where the single RID normally resides in wild-type animals (Fig. 1B,C). These neurons are positioned side by side and exhibit an identical neurite projection pattern. Similar to the RID neuron in wild-type animals, the neurites first project ventrally, but when they reach the ventral cord, instead of looping back dorsally, they project posteriorly along the ventral nerve cord and stop prematurely. Hence, these neurites are missing part of the dendrite loop and the axonal region (Fig. 1B,D,E). The canonical *unc-3* loss-of-function allele *e151* (W309 to opal stop) exhibits the same defects of RID duplication and neurite projection (Fig. 1C,D,E). *xd86*, which has the earliest stop codon and highest penetrance defects, was used in the remainder of our study.

All other cells that express the P*ceh-10*::wCherry marker, including AIY and CAN, appear normal with respect to soma number and axon projection in *unc-3* mutants (Fig. 1B). Similarly, with a pan-neuronal marker, the majority of motor neurons appear unaffected with respect to number and dorsal projections, although they exhibit defective migration and defasciculation in the ventral nerve cord as reported previously (Wightman et al., 1997; Prasad et al., 1998) (data not shown). Together, these data suggest that *unc-3* functions in a lineage-restricted manner to affect the number of RID neurons and the pattern of dorsal-ventral RID neurite guidance.

UNC-3 is non-essential for RID terminal differentiation

We next investigated the underlying cause of RID duplication and defective neurite projection. UNC-3 is a terminal selector

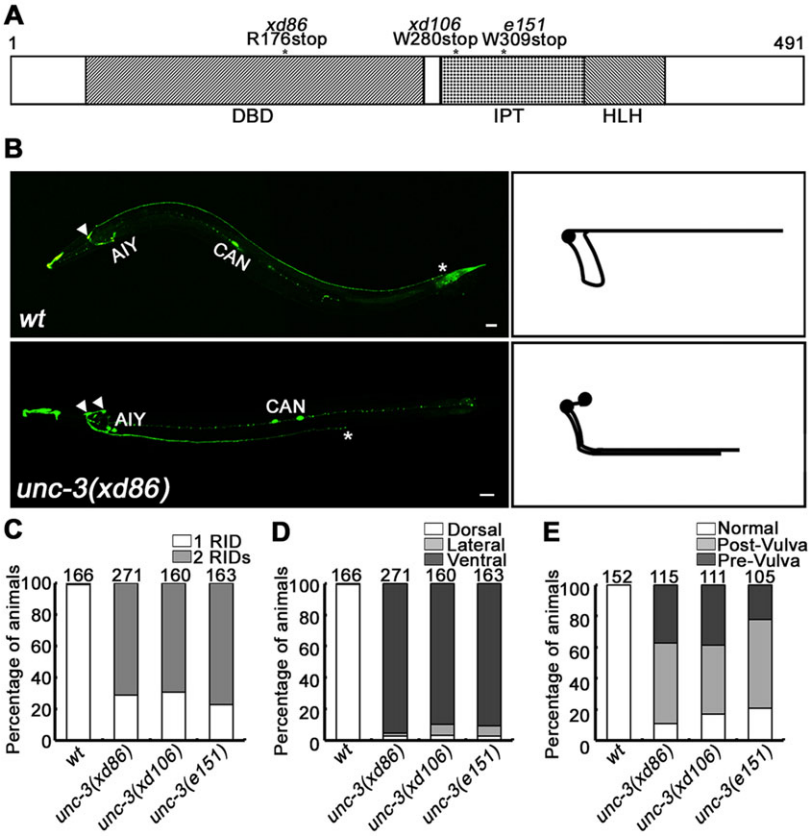

Fig. 1. UNC-3 affects the development of the RID cell lineage. (A) The predicted domain organization of UNC-3. The molecular lesions in the *xd86*, *xd106* and *e151* alleles are indicated with asterisks. DBD, DNA-binding domain; IPT, immunoglobulin-like/plexin/transcription factor domain; HLH, helix-loop-helix domain. (B) Fluorescent images of young adult worms labeled by P*ceh-10*::GFP and schematics of RID in the wild type (wt) and *unc-3* mutants. Arrowheads indicate the cell bodies of RID neurons. AIY and CAN neuron cell bodies are also indicated. Asterisks indicate the termini of RID axons. Anterior is to the left and dorsal is up. Scale bars: 10 µm. (C-E) Quantification of RID duplication (C), dorsal-ventral guidance defects (D) and anterior-posterior outgrowth defects (E) in different *unc-3* mutants. The number of animals scored is indicated above each bar.

Development (2015) 142, 1-11 doi:10.1242/dev.119479

for a fraction of cholinergic motor neurons and sensory neurons (Kim et al., 2005; Kratsios et al., 2012). We first examined whether the RID fate is altered in *unc-3* mutants. We examined the expression of several terminal differentiation markers (*kal-1*, *zig-5*, *ser-2* and *lim-4*) that are activated in various neuronal groups that overlap in RID (Tsalik et al., 2003). All are expressed in the pair of RID-like neurons in *unc-3* mutants (Fig. 2A,D), suggesting that the RID fate is probably unaltered and that this neuron represents a duplication of RID fate. The neurite morphology of the RID-like neurons in *unc-3* mutants partially resembles that of ALA and AVJ(H) neurons, raising the possibility that one or both of the RID-like neurons might also acquire some traits of ALA or AVJ(H). However, neither the ALA marker P*ida-1*::GFP (Zahn et al., 2004) nor the AVJ(H) marker P*flp-12*::GFP (Kim and Li, 2004) was misexpressed in RID neurons in *unc-3* mutants (Fig. 2B-D). Therefore, the RID-like neurons in *unc-3* mutants do not exhibit obvious fate transformation.

Next, we examined whether UNC-3 is sufficient to induce RID fate in other neuronal lineages. Consistent with the role of UNC-3 as a terminal selector for cholinergic motor neurons (Kratsios et al., 2012), ectopic expression of UNC-3 in glutamatergic mechanosensory neurons (PVM and PLM) was sufficient to induce the expression of cholinergic markers *Pacr-14*::DsRed and *Pacr-2*::GFP (Fig. 2E-G). By contrast, ectopic expression of UNC-3 in PVMs did not activate the RID marker P*ceh-10*::wCherry (Fig. 2G). Together, these results indicate that, like the LIM homeodomain protein LIM-4, which is required for some but not all aspects of RID neuron differentiation (Tsalik et al., 2003), UNC-3 is required for several aspects of RID development, including correct number and some aspects of neurite guidance, but is largely dispensable for RID terminal differentiation.

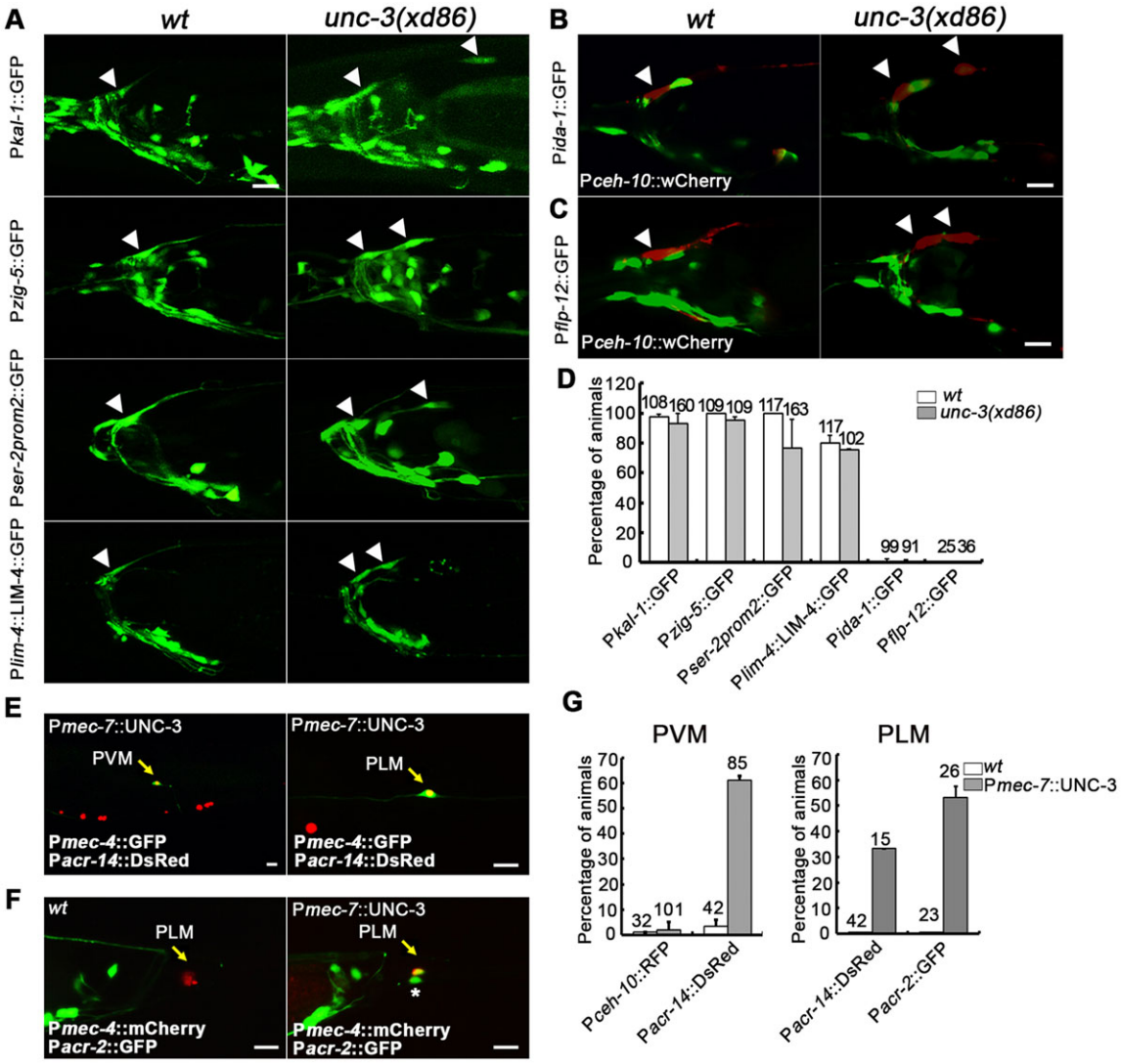

Fig. 2. UNC-3 is non-essential for RID terminal differentiation. (A-C) Expression of (A) different RID markers, (B) the ALA neuronal marker P*ida-1*::GFP and (C) the AVJ (H) neuronal marker P*flp-12*::GFP in wild type and *unc-3* mutants. Arrowheads indicate the cell bodies of RID neurons. (D) Quantification of animals expressing GFP markers in RID neurons in A-C. (E) Expression of the cholinergic marker P*acr-14*::DsRed in PVM and PLM neurons with ectopic expression of UNC-3. (F) Expression of the cholinergic marker P*acr-2*::GFP in PLM neurons with ectopic expression of UNC-3. Asterisk indicates a putative P*acr-2*::GFP-positive PLM neuron that has lost the expression of P*mec-4*::mCherry. (G) Quantification of animals expressing P*ceh-10*::wCherry, P*acr-14*::DsRed or P*acr-2*::GFP in PVM or PLM neurons when UNC-3 is ectopically expressed. The number of animals scored is indicated. For all images, anterior is to the left and dorsal is up. Error bars indicate s.d. Scale bars: 10 µm.

Development (2015) 142, 1-11 doi:10.1242/dev.119479

UNC-3 activates apoptosis in the RID lineage

Next, we address how the functional loss of UNC-3 leads to the development of an ectopic RID neuron. During embryogenesis, the RID lineage precursor ABalappaa divides to give birth of ABalappaaa, which dies, and ABalappaap, which is the RID precursor. Shortly after the division of ABalappaap, the posterior daughter ABalappaapp undergoes apoptosis, whereas the anterior progeny becomes RID (Fig. 3A). HAM-1, a protein with a winged helix DNA-binding motif, is required for the proper division of the RID precursor ABalappaap and subsequently activates apoptosis in one of its two progenies (Guenther and Garriga, 1996; Frank et al., 2005). In *ham-1(n1438)* mutants, 48% of worms have two RID neurons and 10% have three or four RIDs (Fig. 3B). The apoptotic activator EGL-1 and the pro-caspase CED-3 are both required for RID sister cell apoptosis, as 90% of *egl-1* and 80% of *ced-3* mutant animals show RID duplication (Fig. 3B). Unlike in *unc-3* mutants, RID-like neurons in *ham-1*, *egl-1* and *ced-3* mutants all exhibit wild-type neurite projections.

Two apoptosis events occur in the RID lineage: the sister of the RID precursor and the sister of RID. Since *unc-3* mutants show duplicated, but not three or four, RID neurons, it is possible that UNC-3 restricts RID number by activating apoptosis in the RID sister cell. Consistent with this possibility, *unc-3(xd86);ced-3(n717)* and *unc-3(xd86);egl-1(n3082)* double mutants did not exhibit significant enhancement in the penetrance of RID duplication when compared with either single mutant (Fig. 3B). In *unc-3(xd86); ham-1(n1438)* double mutants, however, 28% of animals have three or even four RIDs, as compared with 10% in *ham-1(n1438)* single mutants. A similar trend of enhancement was observed in *egl-1(n3082);ham-1(n1438)* double mutants (Fig. 3B). These results indicate that HAM-1 may affect the division of both precursor cells, i.e. ABalappaa and ABalappaap, in the RID lineage. The extra one or two RIDs in *ham-1* mutants might result from the survival of ABalappaaa (the sister of the RID precursor) or its fate transformation to that of ABalappaap (the RID precursor). Thus, it appears that *ham-1* affects RID number through affecting the division pattern of the RID lineage precursor, whereas *unc-3* mutations cause RID duplication due to a failure to activate apoptosis in the RID sister.

We further examined whether UNC-3 plays a ubiquitous role in apoptosis in other neuronal lineages. The birth of RMEL/R, ASEL/R, RIML/R and ASIL/R, like that of RID, involves apoptosis of their sister cells after the final round of cell division. These neurons exhibit normal number and morphology in *unc-3* mutants (Fig. 3C). There is no significant difference in total cell death corpse number in the comma or 1.5-fold stage embryo in *unc-3* mutants as compared with wild-type embryos (data not shown). Taken together, our results indicate that UNC-3 affects apoptosis in a lineage-specific manner.

UNC-3 is expressed and functionally required in the RID lineage

To examine where UNC-3 functions, we monitored the embryonic and postembryonic expression of a functional *unc-3* fosmid reporter

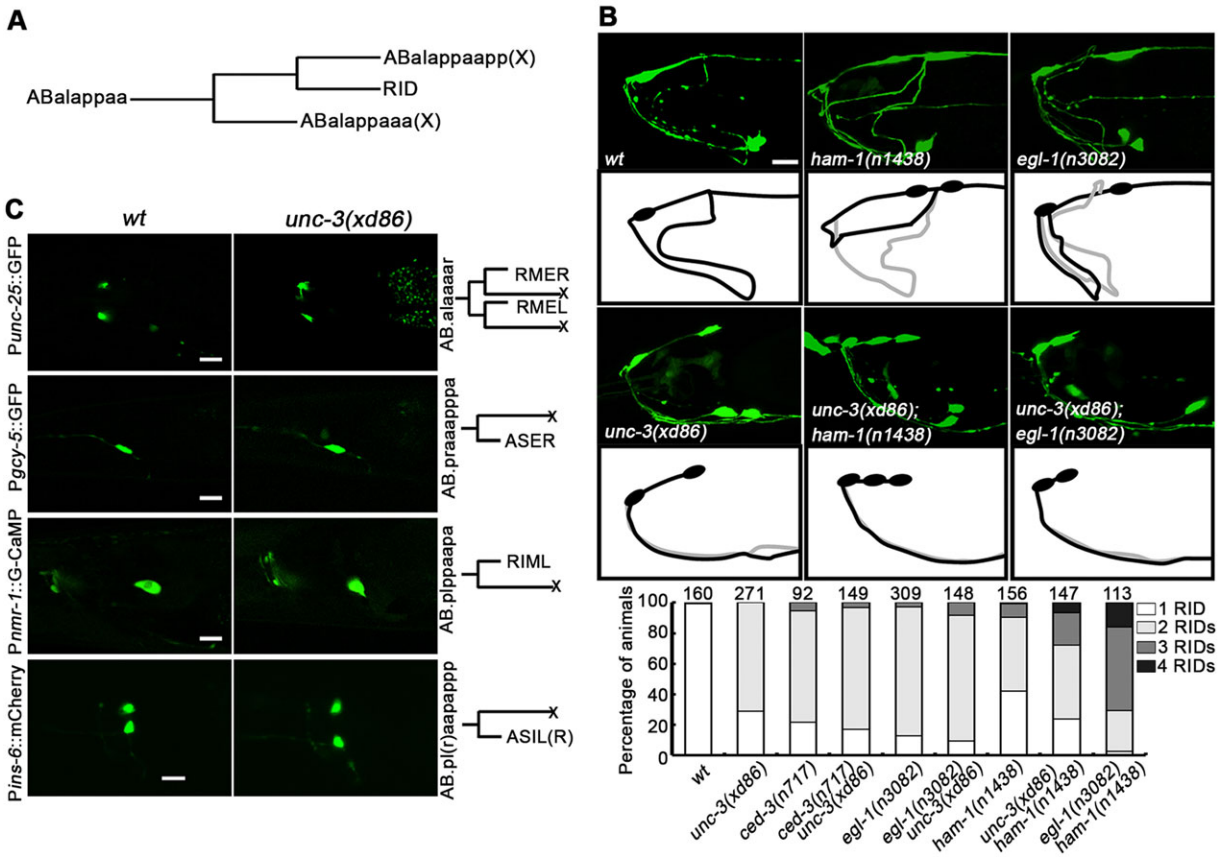

Fig. 3. UNC-3 activates apoptosis in the RID lineage. (A) The cell lineage of RID. (B) Fluorescence images of the P*ceh-10*::GFP reporter and schematics of RID in wild type, *ham-1(n1438)*, *egl-1(n3082)*, *unc-3(xd86)*, *unc-3(xd86);ham-1(n1438)* and *unc-3(xd86);egl-1(n3082)*. Quantification of RID neuron numbers in each genetic background is shown. The number of animals scored is indicated. (C) Expression of RME, ASE, RIM and ASI markers in wild type and *unc-3* mutants. The cell lineages of RME, ASE, RIM and ASI neurons are illustrated alongside. (A,C) X indicates apoptotic cell. Scale bars: 10 µm.

Development (2015) 142, 1-11 doi:10.1242/dev.119479

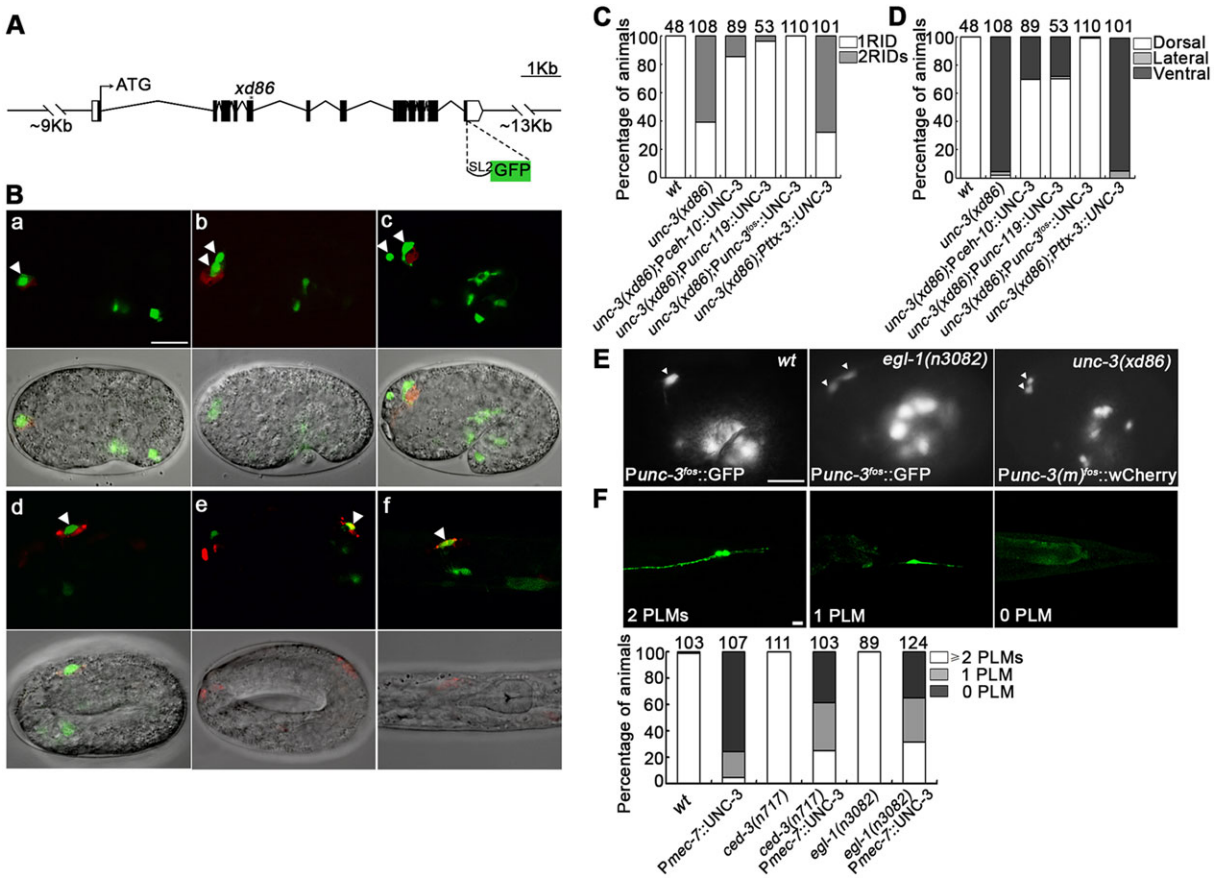

Fig. 4. UNC-3 is expressed and functions in the RID lineage. (A) Genomic structure of the *unc-3* fosmid reporter. The *xd86* mutation is indicated with an asterisk. The position of the GFP insertion is shown. (B) The *unc-3* fosmid-based reporter is expressed in the RID lineage at different stages during the development of RID: (a) pre-comma stage; (b) comma stage; (c) 1.5-fold stage; (d) 3-fold stage; (e) 4-fold stage; (f) L1 stage. Green fluorescence, P*unc-3*^{fos}::GFP; red fluorescence, P*ceh-10*::wCherry. Bright-field and fluorescence images are merged in the lower panels. (C,D) Rescue of RID number (C) and dorsal-ventral guidance (D) defects in *unc-3(xd86)* mutants by different transgenes. (E) RID in wild type, *egl-1* and *unc-3* mutants at the 1.5-fold stage visualized with the P*unc-3*^{fos}::GFP or P*unc-3(m)*^{fos}::wCherry reporter. (B,E) Arrowheads indicate RID neurons and/or RID sister cells. Anterior is to the left and dorsal is up. (F) Ectopic expression of UNC-3 in PLM neurons results in the loss of PLM. Fluorescence images of animals with two PLMs, one PLM, or no PLM visualized with the P*mec-4*::GFP reporter. Quantification of the number of PLM neurons in the different backgrounds is shown. The number of animals scored is indicated. Scale bars: 10 µm.

that contains a bi-cistronic GFP reporter at the C-terminus of the UNC-3 coding sequence (Fig. 4A,B). This reporter fully rescued the RID phenotypes of *unc-3* mutants (Fig. 4C,D).

During embryogenesis, at the pre-comma stage, the GFP signal was first observed in the RID precursor (ABalappaap) before its final round of cell division. After the division, GFP signals were observed in both progenies. After the RID sister cell had undergone programmed cell death, the RID terminal differentiation marker P*ceh-10*::wCherry was observed in the surviving cell. Co-expression of the *ceh-10* and *unc-3* reporters in the RID neuron persisted into the larval stage (Fig. 4B). Similar to what has been reported previously (Prasad et al., 1998, 2008; Kratsios et al., 2012), the *unc-3* fosmid reporter also exhibited expression in cholinergic motor neurons (data not shown).

Since the *unc-3* fosmid reporter was expressed prior to the *ceh-10* reporter in the RID lineage, we further compared RID development in *egl-1(n3082)* and *unc-3(xd86)* mutants using a functional *unc-3* fosmid reporter and one that carries the *xd86* mutation, respectively. In both mutants, the two RID-like neurons appeared at a similar developmental stage, which suggests that the ectopic RID neuron in *unc-3* mutants is unlikely to be caused by a reiterative defect (Fig. 4E). These results further rule out the possibility that the ectopic RID neuron in *unc-3* mutants results from fate transformation from other lineages.

The expression of the *unc-3* fosmid reporter in the RID lineage is consistent with a functional requirement of UNC-3 for RID development. Indeed, restoring UNC-3 expression in *unc-3* mutants in all neurons using a pan-neuronal promoter (P*unc-119*), or in a restricted subgroup of neuron lineages including RID (P*ceh-10*), restored both the number and neurite morphology of the RID neuron. As a control, expressing UNC-3 in AIY neurons did not rescue the *unc-3* mutant RID phenotype (Fig. 4C,D). This suggests a cell-autonomous role of UNC-3 in the RID lineage. In two *unc-3* embryos in which one ectopic RID was ablated, both animals exhibited neurite trajectory defects in the surviving RID neuron (data not shown), further supporting a cell-autonomous role of UNC-3. Moreover, loss of the ectopic RID sister in *unc-3* mutants by *Pceh-10*-driven UNC-3 expression suggests that UNC-3 is able to promote apoptosis in the RID sister cell even past the normal developmental time window.

The lineage-specific involvement of UNC-3 in apoptosis along with the restricted expression pattern of UNC-3 raise the question of whether UNC-3 could induce ectopic apoptosis in other lineages. The PLMs, which are a pair of mechanosensory neurons derived embryonically, are widely used to analyze ectopic apoptotic activity

Development (2015) 142, 1-11 doi:10.1242/dev.119479

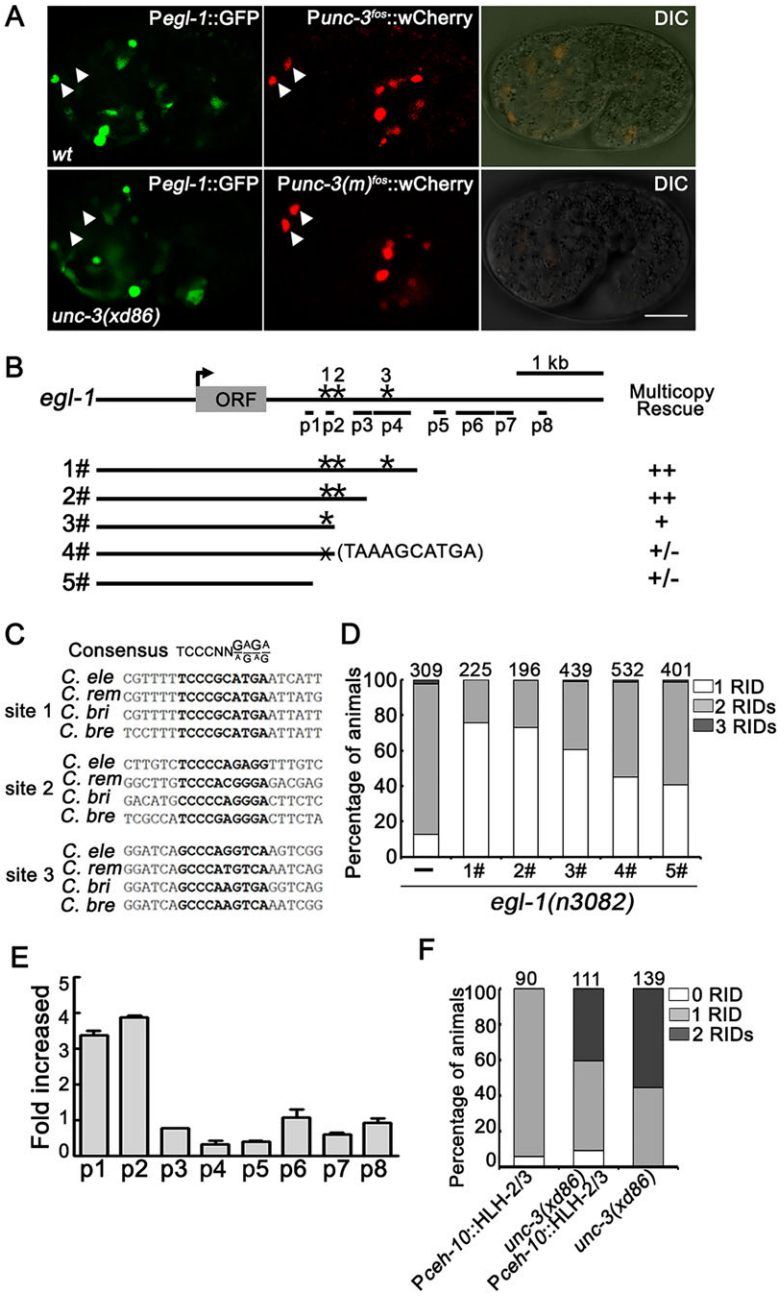

Fig. 5. UNC-3 promotes apoptosis of the RID sister cell and affects the expression of *egl-1*. (A) P*egl-1*::GFP in wild type and *unc-3* mutants. Green fluorescence, P*egl-1*::GFP reporter; red fluorescence, P*unc-3*^{fos}::wCherry in wild type and P*unc-3(m)*^{fos}::wCherry in *unc-3(xd86)* mutants. Arrowheads indicate RID neurons and/or RID sister cells. Anterior is to the left and dorsal is up. Scale bar: 10 µm. (B) The genomic structure of *egl-1* and the different genomic DNA fragments used for the *egl-1* rescue assay. The gray box indicates the *egl-1* open reading frame (ORF). Asterisks indicate the location of three evolutionarily conserved potential UNC-3 binding sites (sites 1, 2 and 3). Short lines indicate the regions used in ChIP analysis. (C) Alignment of the three putative UNC-3 binding sites in different *Caenorhabditis* species. (D) Quantification of RID neuron numbers in the *egl-1(n3082)* mutant with and without transgenes carrying different *egl-1* fragments. (E) ChIP-qPCR results show that UNC-3 binds to the p1 and p2 regions. Error bars represent s.d. (F) Quantification of RID neuron numbers in different genetic backgrounds. The number of animals scored is indicated.

(Wang et al., 2002). When UNC-3 was ectopically expressed in these mechanosensory neurons, 95% of the transgenic animals lost P*mec-4*::GFP reporter expression in one or both PLMs (Fig. 4F). The loss of reporter expression might be due to ectopic cell death or altered PLM fate. PLM marker expression was partially restored by the *egl-1* or *ced-3* mutation (Fig. 4F), suggesting that ectopic expression of UNC-3 was able to induce cell death. The incomplete suppression by *egl-1* or *ced-3* might reflect an altered fate of the surviving PLM neurons. Indeed, in some transgenic animals we noted the presence of ectopic P*acr-2*::GFP-positive neurons where PLMs normally reside, consistent with their transformation to a cholinergic fate (Fig. 2F).

EGL-1 expression is abolished in the RID sister cell in *unc-3* mutants

Several transcription factors promote or suppress cell type-specific apoptosis through regulating expression of the apoptotic gene *egl-1* (Nehme and Conradt, 2008). We examined whether UNC-3 regulates apoptosis of the RID sister cell by affecting *egl-1* expression. In 30 out of 32 wild-type embryos examined, a P*egl-1*::GFP reporter (*smIs89*) was expressed in the RID sister cell shortly after the division of its precursor (Fig. 5A), which coincided with its apoptosis. By contrast, 28 out of 30 *unc-3* embryos failed to activate the P*egl-1*::GFP reporter in the RID lineage (Fig. 5A). The gross expression pattern of *Pegl-1*::GFP was similar in wild-type and *unc-3* embryos, suggesting that *unc-3* mutation does not globally block reporter expression. Together, these results indicate that UNC-3 is required for *egl-1* expression in, and subsequent apoptosis of, the RID sister.

Since UNC-3 is a transcription factor, we explored the possibility that it directly activates *egl-1* expression. We first sought to identify the minimal cis DNA element required for *egl-1* rescue activity in RID sister cells. Because the P*egl-1*::GFP reporter has a short promoter (~1 kb) and long 3′ downstream region (~6 kb), we

Development (2015) 142, 1-11 doi:10.1242/dev.119479

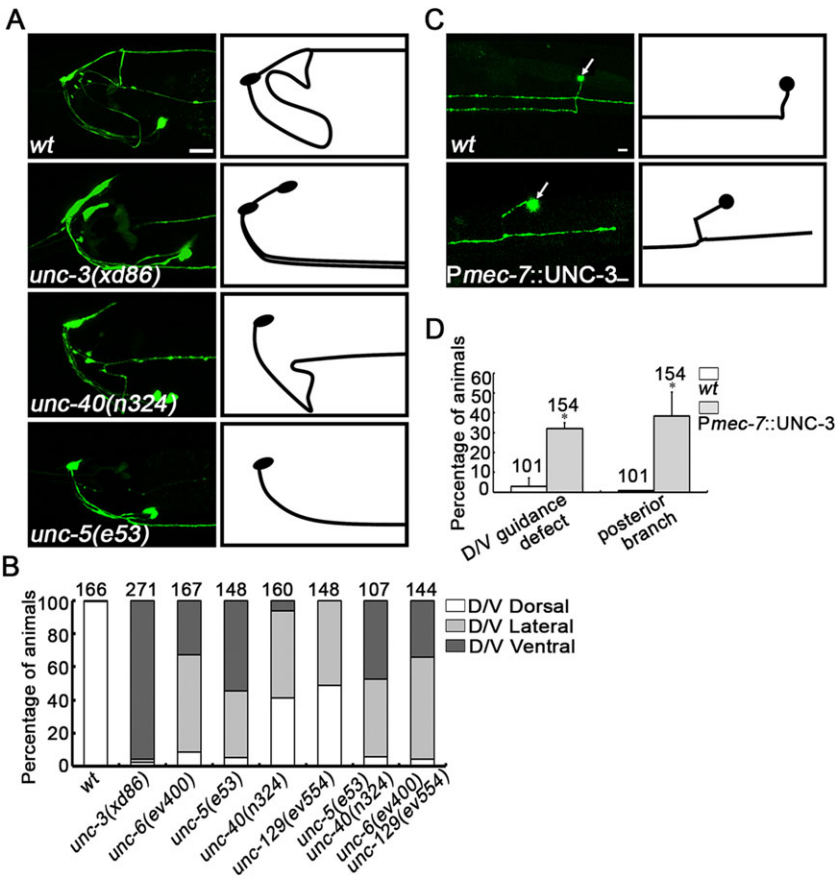

Fig. 6. UNC-3 regulates RID axon projection. (A) Fluorescence images of the P*ceh-10*::GFP reporter and schematics of RID in wild type, *unc-3(xd86)*, *unc-40 (n324)* and *unc-5(e53)* showing the dorsal-ventral guidance defects. (B) Quantification of RID dorsal-ventral guidance defects in different mutants. (C) Outgrowth of PVM neurons visualized with the P*mec-4*::GFP reporter in wild type and in animals overexpressing *Pmec-7::*UNC-3. UNC-3 overexpression leads to dorsal-ventral guidance and posterior branch phenotypes of PVM neurons. Arrows indicate soma of PVM neurons. (D) Quantification of guidance defects in C. The number of animals scored is indicated. Error bars represent s.d. **P*<0.05 (Student's *t*-test).

generated *egl-1* genomic fragments with various lengths of 3′ downstream region (Fig. 5B) and tested their ability to restore RID number in *egl-1(n3082)* mutants. The most significant reduction in rescuing activity occurred when a 1.2 kb 3′ downstream region was removed (Fig. 5B,D, compare constructs 1# and 5#).

Both mammalian COE proteins and *C. elegans* UNC-3 bind to a conserved COE binding motif (TCCCNN$^{G}/_{A}/^{G}/_{A}/^{G}/_{A}$) to regulate target gene transcription (Wang et al., 1993; Kim et al., 2005; Kratsios et al., 2012). Within this 1.2 kb *egl-1* fragment, we identified two putative COE binding sites (sites 1 and 2) and a less stringent binding site (site 3), which are conserved among the *C. elegans*, *C. remanei*, *C. briggsae* and *C. brenneri* genomes (Fig. 5B,C). Deleting site 3 (construct 2#) did not affect rescue activity (Fig. 5B,D), whereas further removing a region containing site 2 (construct 3#) partially impairs rescue activity; moreover, point mutations that disrupt site 1 (construct 4#) further reduced rescue activity (Fig. 5B,D). Together, this suggests that putative COE binding sites 1 and 2 might act redundantly in mediating UNC-3-dependent *egl-1* activation in the RID sister. To examine whether UNC-3 can physically bind these sites, we performed ChIP analysis with a FLAG-tagged full-length UNC-3 fusion protein. Compared with other regions tested, a strong binding signal was detected around sites 1 and 2 (Fig. 5E). Together, these results suggest that UNC-3 may regulate the expression of *egl-1* in RID sister cells through multiple binding sites. We note that all our functional *egl-1* constructs, including construct 1#, required multi-copy transgenic array for rescue (Fig. 5B; data not shown). Therefore, there might be other elements, regulated by UNC-3 or other transcription factors, that control *egl-1* expression in the RID lineage.

If UNC-3 promotes apoptosis of the RID sister by activating *egl-1* expression, then forced reactivation of *egl-1* expression should bypass the requirement for *unc-3* in the RID lineage. HLH-2 and HLH-3 promote *egl-1* expression in the NSM neuron and its sister (Thellmann et al., 2003). Ectopic HLH-2 and HLH-3 expression in the RID lineage (P*ceh-10*::HLH-2 and P*ceh-10*::HLH-3) resulted in ∼6% RID loss, presumably due to ectopic RID cell death (Fig. 5F). Introducing the same transgene into *unc-3* mutants decreased the two RID neuron phenotype from ∼60% to 40% (Fig. 5F). These results support the hypothesis that UNC-3 promotes *egl-1* expression in the RID sister to promote its death.

UNC-3 regulates aspects of RID neurite projection

In both *egl-1* and *ced-3* mutants, the duplicated RID neurons exhibit normal axon trajectories. This is in contrast to *unc-3* mutants, in which the pair of RID neurons exhibit both dorsal-ventral and anterior-posterior neurite outgrowth defects (Fig. 1B). This suggests that, in addition to triggering EGL-1-mediated apoptosis in the RID lineage, UNC-3 plays roles in neuronal differentiation, probably through different effectors.

Several guidance signals, including Netrin/UNC-6 and its receptors DCC/UNC-40 and UNC-5, and UNC-129/TGFβ, are known to contribute to dorsal-ventral neurite guidance and cell migration (Hedgecock et al., 1990; Colavita et al., 1998). The RID neurite exhibited varying degrees of dorsal-ventral guidance defects in *unc-6(ev400)*, *unc-5(e53)*, *unc-40(n324)* and *unc-129(ev554)* single mutants, the combinatorial receptor mutant *unc-5(e53);unc-40(n324)* and the compound guidance cue mutant *unc-6(ev400); unc-129(ev554)*, but none of these defects was as severe as those of *unc-3(xd86)* mutants (Fig. 6A,B). Therefore, additional mechanisms are involved in dorsal-ventral guidance of the RID neurite.

Ectopic expression of UNC-3 could alter the neurite projection pattern in a specific neuronal context. In wild-type animals the PVM

Development (2015) 142, 1-11 doi:10.1242/dev.119479

axon migrates ventrally and, upon reaching the ventral nerve cord, it turns and migrates anteriorly. In more than 30% of transgenic animals ectopically expressing UNC-3 in PVM, the PVM axon first extended anteriorly or posteriorly, prior to growing ventrally. Upon reaching the ventral nerve cord, it often sent a branch posteriorly (Fig. 6C,D). Together, these data suggest that in the RID lineage UNC-3 not only determines the survival states during neurogenesis, but also regulates several aspects of neurite projection during neuronal differentiation.

UNC-3 interacts with the histone acetyltransferase CBP-1/P300 to promote apoptosis and neurite outgrowth

Several UNC-3 co-factors have been identified in various developmental processes, including the histone demethylase JMJD-3.1 for Y cell to PDA redifferentiation and the C2H2 zinc finger protein PAG-3 for VA and VB motor neuron terminal differentiation (Prasad et al., 2008; Zuryn et al., 2014). RID number and neurite pattern were normal in *pag-3(ok488)*, *pag-3(n3098)*, *jmjd-3.1(gk384)* and *jmjd-3.1(gk387)* mutants (data not shown), indicating that UNC-3 may interact with other factors to regulate apoptosis and neurite outgrowth.

We performed a yeast two-hybrid screen to identify additional UNC-3 partners in apoptosis and/or neurite outgrowth. We uncovered UNC-3, consistent with a previous report that UNC-3 forms homodimers (Prasad et al., 2008). In addition, we identified CBP-1, a *C. elegans* histone acetyltransferase P300, which is required for DNA damage-induced apoptosis (Yang et al., 2009). CBP-1 is a large protein; the recovered *cbp-1* clone encodes amino acids 1319-1635, including its two zinc finger domains (Fig. 7A). Using the GST pulldown assay, we confirmed that UNC-3 and the CBP-1 zinc finger region interact directly *in vitro* (Fig. 7B).

cbp-1 is essential for *C. elegans* survival, precluding an analysis of the RID phenotype in null mutants. To explore the role of *cbp-1* in the RID lineage, we took two alternative approaches. First, we reasoned that if binding to UNC-3 is important for CBP-1 function, then overexpression of the UNC-3-binding region of CBP-1 may compete with wild-type CBP-1, causing a dominant-negative effect in wild-type animals. Indeed, overexpression of the CBP-1 zinc finger region using the *Pceh-10* promoter in wild-type animals led to a low penetrance *unc-3*-like RID phenotype: ~30% of transgenic animals displayed two RID-like neurons, with either ventral or lateral growing neurites (Fig. 7C,D). Second, *cbp-1 (ku258)*, which encodes a CBP-1 variant with two amino acid changes that may compete with wild-type CBP-1 for binding partners (Eastburn and Han, 2005), exhibits a similar RID phenotype to that caused by overexpression of the CBP-1 zinc finger region (Fig. 7C,D). By contrast, expression of the cholinergic marker P*unc-17*::GFP is unchanged in *cbp-1(ku258)* mutants (data not shown). Taken together, these results indicate that UNC-3 partners with an alternative C2H2 zinc finger protein, CBP-1, to promote lineage-specific apoptosis and neurite outgrowth in the RID lineage.

DISCUSSION

COE transcription factors have been implicated in the development and differentiation of multiple tissues. UNC-3, the single *C. elegans* COE family transcription factor, specifies the identity of cholinergic motor neurons and ASI sensory neurons, and promotes postembryonic epithelial to neuron transition in the Y cell (Kim et al., 2005; Prasad et al., 2008; Richard et al., 2011; Kratsios et al., 2012). Here we show that UNC-3, in partner with alternate co-factors, acts as a lineage-specific activator of apoptosis in the RID neuron lineage.

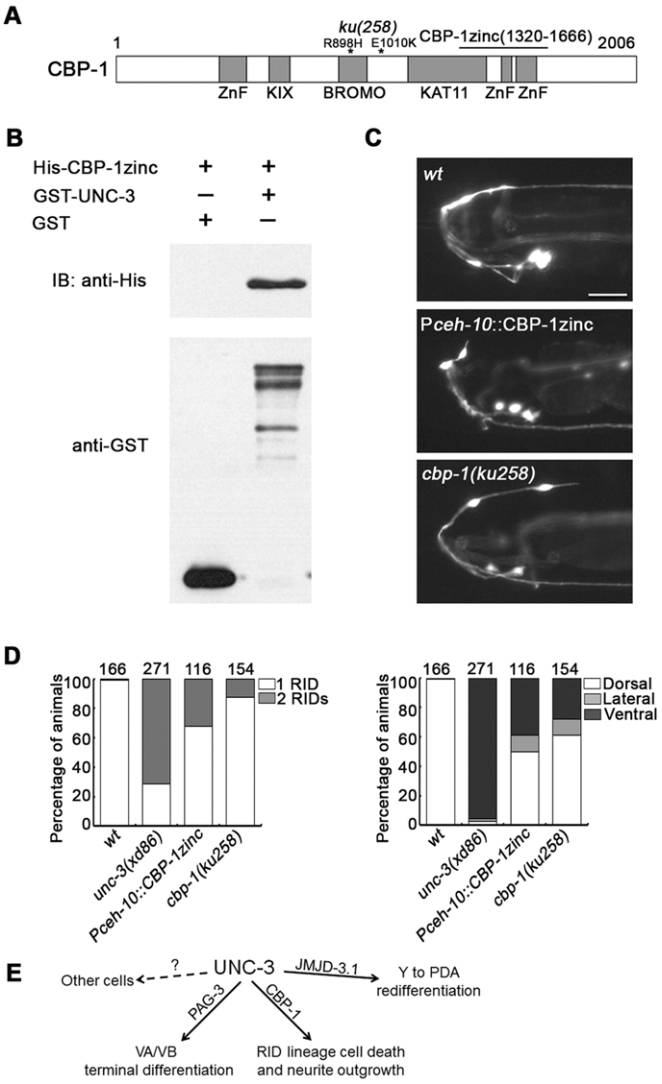

Fig. 7. UNC-3 interacts with the histone acetyltransferase CBP-1 in RID lineage development. (A) The predicted domain organization of CBP-1. ZnF, zinc finger domain; KIX, CREB binding domain; BROMO, bromodomain; KAT11, histone acetyltransferase domain. The protein truncation used in the GST pulldown assay and transgene overexpression is denoted CBP-1zinc. *cbp-1(ku258)* harbors two point mutations. (B) GST pulldown assay showing that UNC-3 can interact with CBP-1zinc. (C) The *cbp-1(ku258)* mutation or overexpression of CBP-1zinc in RID leads to both neurite guidance defects and a two RID phenotype. Anterior is left and dorsal is up. Scale bar: 20 µm. (D) Qualification of RID phenotypes in C. The number of animals scored is indicated. (E) Different co-factors specify the different functions of UNC-3 Besides co-factors in Y/PDA, RID lineage and VA/VB cells, UNC-3 probably functions together with unknown co-factor(s) in other cell types, such as ASI.

UNC-3-dependent apoptosis is part of the lineage program that gives rise to the RID neuron

By interacting with conserved COE binding sites, COE family transcription factors activate or repress the expression of target genes. During B cell development, EBF1 regulates the expression of transcription factors *Pax5*, *Pou2af1* and *Foxo1*, which are required for B cell differentiation (Zandi et al., 2008). EBF1 can also directly regulate the expression of a B cell differentiation marker, *mb-1* (Hagman et al., 1991). Similarly, in *C. elegans*, UNC-3 directly activates terminal differentiation genes (e.g. *unc-17*, *cho-1*), as well as other transcription factors that indirectly inhibit the expression of

Development (2015) 142, 1-11 doi:10.1242/dev.119479

terminal differentiation genes in a subset of motor neurons (Kratsios et al., 2012).

In the RID lineage, with the exception of several aspects of neurite trajectory, UNC-3 is largely dispensable for terminal differentiation. Its dominant role is to ensure apoptosis of the RID sister in order to prevent neuron duplication. An EGL-1 reporter that is transiently activated in the RID sister in wild-type animals fails to be activated in *unc-3* mutants. This finding supports a notion that EGL-1, a shared pro-apoptotic protein, can be activated by multiple lineage-specific transcription factors, instead of by a shared factor in multiple lineages. In this regard, apoptosis might simply represent another lineage specification event that is subject to regulation by lineage-specific transcriptional codes.

Different co-factors specify different functions of COE proteins

During development, transcription factors can be recruited to multiple complexes, where they function with diverse co-factors to activate or repress the transcription of different sets of targets. This allows them to perform distinct functions in multiple cell types. These co-factors include chromatin remodelers, such as histone acetylases, deacetylases, kinases and methylases (Latchman, 1997). The COE transcription factor EBF1, in the presence of the zinc finger protein OAZ/Zfp423 or ZNF521/EHZF, recruits the nucleosome remodeling and histone deacetylase (NuRD) complex to genomic DNA. This leads to reduced accessibility to transcription factors and to the downregulation of target transcription in neuronal precursors and hematopoietic progenitors (Tsai and Reed, 1997; Liao, 2009; Mega et al., 2011). By contrast, in the absence of these co-factors free EBF1 binds the histone acetyltransferase (HAT) p300/CBP and represses its HAT activity, while DNA-bound EBF1 releases p300/CBP, resulting in upregulation of target gene transcription (Zhao et al., 2003). Similar to the partnership between mammalian CBP/p300 and EBF1, we found that CBP-1 is a partner of UNC-3 during RID development. The observation that the UNC-3 co-factors PAG-3 and JMJD-3.1 do not affect RID fate suggests that the lineage-specific function of UNC-3 might be specified through its partnership with different co-factors (Fig. 7E).

UNC-3 expression is observed in both progenies of the RID precursor, but only the RID sister undergoes apoptosis. Other UNC-3-expressing embryonic cells do not undergo apoptosis either. Therefore, although UNC-3 is required for apoptosis, it alone cannot dictate the life-death decision. Thus, there must be another factor(s) that is asymmetrically distributed or that functions differentially between the two progenies to coordinate the RID lineage-specific cell death. This factor either promotes apoptosis in the RID sister with UNC-3, or protects the RID neuron from activating apoptosis by inhibiting *egl-1* expression. CBP-1 is unlikely to be this factor because, like *unc-3*, *cbp-1* affects both RID and the RID sister.

COE transcription factors may have conserved roles in apoptosis and neurite guidance/outgrowth

UNC-3 and mammalian COE transcription factors share over 60% amino acid sequence identity at the DNA-binding (DBD), HLH and IPT domains. A mammalian COE gene, *EBF3*, is either deleted or transcriptionally silenced through methylation in some brain tumors. EBF3 overexpression results in apoptosis by repressing expression of the anti-apoptotic Bcl-2 family protein MCL1 and activating the cleavage of caspase 3 (Zhao et al., 2006). By contrast, another COE factor, EBF1, is required for B cell survival (Gyory et al., 2012). These findings suggest that mammalian COE transcription factors are likely to be involved in the process that determines whether cells survive or die.

Although the UNC-3 target genes responsible for RID neurite guidance/outgrowth remain to be determined, the role of COE genes in neurite guidance/outgrowth is likely to be conserved. Neurite defects have been associated with mutations in COE genes in other organisms. *EBF1* mutation affects the response of facial branchiomotor neurons to the rhombomeric environment and leads to migration defects in these neurons (Garel et al., 2000). *EBF1* inactivation also affects the pathfinding of thalamic and retinal ganglion neurons (Garel et al., 2002; Jin and Xiang, 2011). Inactivation of *EBF2* and *EBF3* leads to the failure of olfactory neurons (ORNs) to project to the dorsal olfactory bulb (Wang et al., 2004). The *Drosophila* COE transcription factor Knot is expressed in class IV multi-dendritic sensory neurons and is essential for the development of their elaborative dendritic arbors (Kieslinger et al., 2005; Hattori et al., 2007). *C. intestinalis* COE rescues the cholinergic marker expression defects of *unc-3* mutants (Kratsios et al., 2012). Consistently, we found that in *unc-3* mutants the anterior-posterior neurite outgrowth defect of RID (but not the soma number or dorsal-ventral guidance defect) was rescued by *C. intestinalis* COE (data not shown). In summary, these findings suggest that COE family protein function is conserved in regulating neurite outgrowth/guidance.

MATERIALS AND METHODS

C. elegans genetics

All strains were maintained on NGM plates at 22°C using standard methods (Brenner, 1974). The wild-type strain was Bristol (N2). Other strains used were as follows. LGI: *unc-40(n324)*, *hpIs162 [*P*ceh-10*::wCherry+*pRF4(rol-6)]*, *zdIs5 [*P*mec-4*::GFP+*lin-15(+)]*; LGII: *inIs179 [*P*ida-1*::GFP*]*, *juIs76 [*P*unc-25*::GFP*]*; LGIII: *otIs264 [*P*ceh-36*::tagRFP*]*, *ynIs82 [*P*flp-12*::GFP*]*; LGIV: *cbp-1(ku258)*, *ced-3(n717)*, *ham-1(n1438)*, *unc-5(e53)*, *unc-129 (ev554)*, *hpIs202 [*P*ceh-10*::GFP+*lin-15(+)]*, *otIs33 [*P*kal-1*::GFP*]*; LGV: *egl-1(n3082)*, *ntIs1 [*P*gcy-5*::GFP+*lin-15(+)]*, *sraIs49 [*P*nmr-1*::G-CaMP +*unc-119(+)]*; LGX: *unc-3(e151)*, *unc-3(xd86)*, *unc-3(xd106)*, *unc-6 (ev400)*. Ex lines and strains without exact chromosome information were: *hpEx2819 [*P*lim-4*::LIM-4::GFP*]*, *hpEx3205 [*P*unc-3*^{fos}::wCherry+P*myo-3*::RFP*]*, *hpEx3206 [*P*unc-3(m)*^{fos}::wCherry+P*myo-3*::RFP*]*, *jxEx30[*P*ins-6*::mCherry+P*ofm-1*::GFP*]*, *otEx536 [*P*ser2prom2*::GFP*]*, *otEx4844 [*P*acr-14 (300bp promoter)*::DsRed2+*pha-1(+)]*, *otIs11 [*P*zig-5*::GFP+*pRF4(rol-6)]*, *smIs89[*P*egl-1*::NLS::GFP*]*, *xdEx902 [*P*mec-7*::UNC-3+*pRF4(rol-6)]*, *xdEx1056 [*P*unc-119*::UNC-3+P*sur-5*::GFP*]*, *xdEx1087 [*P*ceh-10*::UNC-3 +P*sur-5*::GFP*]*, *xdEx1091 [*P*unc-3*^{fos}::GFP+P*sur-5*::RFP*]*, *xdEx1149[*P*ceh-10*::CBP-1zinc*]*, *xdIs61[*P*unc-119*::3xFLAG::UNC-3*]*.

For the EMS screen, *hpIs162* animals were treated with 48 nM EMS, and mutants with an abnormal RID marker expression pattern were isolated in the F2 generation. Approximately 6000 mutagenized haploid genomes were screened and 12 mutants were recovered. *xd86* and *xd106* were mapped to chromosome X. Since both showed uncoordinated and weak coiler phenotypes resembling *unc-3* mutants, we sequenced the entire coding region of the *unc-3* gene by amplifying PCR products from *xd86* and *xd106* animals. A C-to-T mutation at 4036 bp (R176stop) and a G-to-A mutation at 7958 bp (W280stop) downstream of the *unc-3* ATG were found in *xd86* and *xd106*, respectively (Fig. 1A).

Molecular biology and transgenes

To generate rescue constructs, the wild-type *unc-3* cDNA fragment was RT-PCR amplified from N2-derived total RNA and inserted into the *Kpn*I/*Eco*RI sites of *pPD95.77* (kindly provided by Dr Andrew Fire, Stanford University, CA, USA). *unc-119*, *ceh-10* and *ttx-3* promoters were amplified from wild-type genomic DNA and inserted into the multiple cloning sites of *pPD95.77*. To generate FLAG-tagged UNC-3, 3xFLAG sequence was amplified and inserted into the *Kpn*I site of the P*unc-119*::UNC-3 vector. The *unc-3* cDNA was also inserted into *pPD52.102* (kindly provided by Dr

Development (2015) 142, 1-11 doi:10.1242/dev.119479

Andrew Fire) to generate plasmid P*mec-7*::UNC-3. The fosmid-based reporter P*unc-3*^{fos}::GFP was constructed following standard protocols (Tursun et al., 2009). For the *xd86*-mimic mutant form fosmid reporter P*unc-3(m)*^{fos}::wCherry, the *galK* gene flanked by 50 bp of homologous sequence was used to replace 240 bp of the *unc-3* locus surrounding the *unc-3(xd86)* mutation site by recombination. An appropriate PCR product was then amplified from *xd86* genomic DNA and used to replace the *galK* sequence by recombination. The cDNA of HLH-2, HLH-3 or the CBP-1 zinc finger region was amplified from N2-derived cDNA and inserted into the *ceh-10* promoter-containing vector to generate P*ceh-10*::HLH-2, P*ceh-10*::HLH-3 and P*ceh-10*::CBP-1zinc constructs, respectively. For *egl-1* rescue fragments, various lengths of *egl-1* genomic DNA were amplified from N2. Site-directed mutagenesis was performed to mutate specific nucleotides within the putative UNC-3 binding sites.

Transgenic lines were generated by microinjection of the indicated constructs or PCR products at 5-50 ng/µl together with transformation markers at 50-100 ng/µl. Co-injection markers were plasmid *pRF4* (kindly provided by Dr Andrew Chisholm, University of California, San Diego, USA) containing the dominant marker *rol-6(su1006)*, or one of the following fluorescent markers: P*sur-5*::RFP, P*sur-5*::GFP, P*myo-2*::RFP or P*myo-3*::RFP.

Image collection and phenotype quantification

Young adult worms and embryos were mounted on dried 2% agarose pads and immersed in M9 buffer with or without 30 mM NaN_3. Images were taken using a Zeiss compound microscope or a Nikon Eclipse confocal microscope. To quantify the RID duplication defects, neurite guidance defects and fluorescent marker expression levels, young adult worms were mounted and then examined by fluorescence microscopy. For the dorsal-ventral guidance defects, we categorized worms as defective if either one of the two RIDs had a dorsal-ventral defect. For the anterior-posterior defects, we quantified the RID neuron with the longer axon.

Yeast two-hybrid screen

The yeast transformation procedure was conducted using standard techniques. A full-length *unc-3* cDNA was inserted into *pBTM116* (containing the LexA DNA-binding domain for Leu selection; kindly provided by Dr Andrew Chisholm). An UNC-3 fusion protein with the DNA-binding domain was used as bait to screen a *C. elegans* mixed stage cDNA library. Yeast bearing both UNC-3 and the potential interactors were seeded onto –Leu –Trp –His plates containing 2.5 mM 3-amino-1,2,4-triazole (3AT). Clones grown on –Leu –Trp –His plates were further tested for their ability to produce β-galactosidase. Positive clones were analyzed by DNA sequencing.

Chromatin preparation and immunoprecipitation

The FLAG-tagged UNC-3 transgenic strain (*xdIs61*) was grown in a liquid culture at 20°C. Adult worms were bleached [1.5 M NaOH, 12% NaOCl (v/v)] to collect embryos. These embryos were treated with 2% formaldehyde in PBS for 30 min at room temperature to allow cross-linking, before the reaction was quenched with 125 mM glycine for 15 min. Treated embryos were washed four times with PBS containing 1 mM PMSF. The embryos were homogenized with a cordless motor and then resuspended in FA buffer [50 mM HEPES/KOH pH 7.5, 1% Triton X-100, 1 mM EDTA, 0.1% sodium deoxycholate, 150 mM NaCl, 1 mM PMSF, 20 mM DTT, Protease Inhibitor Cocktail (Roche)] and the chromatin was sheared to 100-1000 bp range by sonication (30% amplitude, 10 s on, 59 s off, repeat 35 times). Cellular debris was removed by centrifugation at 13,000 rpm (15,700 ***g***) for 15 min at 4°C, and the supernatant was used for chromatin immunoprecipitation (ChIP). The samples were pre-cleared with protein A- and protein G-agarose beads (Millipore), then incubated with anti-FLAG antibody (Sigma) at 4°C overnight prior to a 2 h incubation with protein A- and protein G-agarose beads. Bound DNA in the beads was eluted and purified using a DNA purification kit (Dongsheng Biotech), then quantified by real-time PCR using the indicated *egl-1* primer sets. Results were plotted as fold-enrichment of anti-FLAG immunoprecipitation versus input. The following primers were used: p1f, 5'-cggtagcctaaggaatggaa-3′; p1r, 5′-acgtggatggcattgttaga-3′; p2f, 5′-tggggagacaagtcaagaca-3′; p2r, 5′-aattgtgcgtacccaatctg-3′; p6f, 5′-gtaacgggcaaatagcgggc-3′; and p6r, 5′-acctttgaacgtcgtttcc-3′. Sequences of other primer sets can be found in Table S1 in the supplementary material. Primer set p6 was chosen as an internal control.

Protein expression and GST pulldown

The *cbp-1zinc* cDNA corresponding to amino acids 1320-1666 of CBP-1 was cloned into *pET28c* vector (Novagen) to generate an N-terminal His tag fusion. Full-length *unc-3* was cloned into *pGEX-4T-1* vector (GE Healthcare) to generate an N-terminal GST tag fusion. These constructs were expressed in *E. coli* BL21(DE3) cells with 0.5 mM IPTG at 18°C. The cells were collected and resuspended in lysis buffer [1× PBS, 1% NP40, 1 mM PMSF, 20% glycerol (v/v)], and then lysed by sonication. His-tagged CBP-1zinc protein with GST-tagged UNC-3 or GST alone was incubated with glutathione-Sepharose beads (GE Healthcare) in lysis buffer at 4°C overnight. The beads were washed with lysis buffer three times, and then boiled for 10 min in SDS-PAGE sample loading buffer. The CBP-1zinc protein was detected by His antibody (1:4000, Abcam).

Acknowledgements

We thank Drs Oliver Hobert, Xiaochen Wang, Chonglin Yang and the Caenorhabditis Genetics Center for strains and reagents; Drs Guangshuo Ou and Yongping Chai for live image analysis; Dr Helen McNeill for use of the image facility; and Dr Chonglin Yang for critical reading of the manuscript.

Competing interests

The authors declare no competing or financial interests.

Author contributions

X.H. and M.Z. conceived and supervised the study. M.D. provided guidance in designing the experiments. J.W., Q.G.. W.W. and X.L. performed the experiments. J.C. and V.L. provided reagents. J.W., M.D., M.Z. and X.H. analyzed the results. J.W., M.Z. and X.H. prepared the manuscript.

Funding

This work was supported by the National Nature Science Foundation of China [31325018 and 81061120519], the Strategic Priority Research Program of the Chinese Academy of Sciences [XDB13030300], the Chinese Academy of Sciences [KSCX-EW-R-05] to X.H.; and the Canadian Institute of Health Research [CCI-109618] to M.Z.

Supplementary material

Supplementary material available online at
http://dev.biologists.org/lookup/suppl/doi:10.1242/dev.119479/-/DC1

References

Akerblad, P., Lind, U., Liberg, D., Bamberg, K. and Sigvardsson, M. (2002). Early B-cell factor (O/E-1) is a promoter of adipogenesis and involved in control of genes important for terminal adipocyte differentiation. *Mol. Cell. Biol.* **22**, 8015-8025.

Brenner, S. (1974). The genetics of Caenorhabditis elegans. *Genetics* **77**, 71-94.

Colavita, A., Krishna, S., Zheng, H., Padgett, R. W. and Culotti, J. G. (1998). Pioneer axon guidance by UNC-129, a C. elegans TGF-beta. *Science* **281**, 706-709.

Conradt, B. (2009). Genetic control of programmed cell death during animal development. *Annu. Rev. Genet.* **43**, 493-523.

Conradt, B. and Horvitz, H. R. (1998). The C. elegans protein EGL-1 is required for programmed cell death and interacts with the Bcl-2-like protein CED-9. *Cell* **93**, 519-529.

Conradt, B. and Horvitz, H. R. (1999). The TRA-1A sex determination protein of C. elegans regulates sexually dimorphic cell deaths by repressing the egl-1 cell death activator gene. *Cell* **98**, 317-327.

Crozatier, M. and Vincent, A. (1999). Requirement for the Drosophila COE transcription factor Collier in formation of an embryonic muscle: transcriptional response to notch signalling. *Development* **126**, 1495-1504.

Danial, N. N. and Korsmeyer, S. J. (2004). Cell death: critical control points. *Cell* **116**, 205-219.

Denning, D. P., Hatch, V. and Horvitz, H. R. (2013). Both the caspase CSP-1 and a caspase-independent pathway promote programmed cell death in parallel to the canonical pathway for apoptosis in Caenorhabditis elegans. *PLoS Genet.* **9**, e1003341.

Eastburn, D. J. and Han, M. (2005). A gain-of-function allele of cbp-1, the Caenorhabditis elegans ortholog of the mammalian CBP/p300 gene, causes an increase in histone acetyltransferase activity and antagonism of activated Ras. *Mol. Cell. Biol.* **25**, 9427-9434.
Ellis, H. M. and Horvitz, H. R. (1986). Genetic control of programmed cell death in the nematode C. elegans. *Cell* **44**, 817-829.
Ellis, R. E., Yuan, J. and Horvitz, H. R. (1991). Mechanisms and functions of cell death. *Annu. Rev. Cell Biol.* **7**, 663-698.
Frank, C. A., Hawkins, N. C., Guenther, C., Horvitz, H. R. and Garriga, G. (2005). C. elegans HAM-1 positions the cleavage plane and regulates apoptosis in asymmetric neuroblast divisions. *Dev. Biol.* **284**, 301-310.
Garel, S., Marin, F., Grosschedl, R. and Charnay, P. (1999). Ebf1 controls early cell differentiation in the embryonic striatum. *Development* **126**, 5285-5294.
Garel, S., Garcia-Dominguez, M. and Charnay, P. (2000). Control of the migratory pathway of facial branchiomotor neurones. *Development* **127**, 5297-5307.
Garel, S., Yun, K., Grosschedl, R. and Rubenstein, J. L. R. (2002). The early topography of thalamocortical projections is shifted in Ebf1 and Dlx1/2 mutant mice. *Development* **129**, 5621-5634.
Guenther, C. and Garriga, G. (1996). Asymmetric distribution of the C. elegans HAM-1 protein in neuroblasts enables daughter cells to adopt distinct fates. *Development* **122**, 3509-3518.
Gyory, I., Boller, S., Nechanitzky, R., Mandel, E., Pott, S., Liu, E. and Grosschedl, R. (2012). Transcription factor Ebf1 regulates differentiation stage-specific signaling, proliferation, and survival of B cells. *Genes Dev.* **26**, 668-682.
Hagman, J., Travis, A. and Grosschedl, R. (1991). A novel lineage-specific nuclear factor regulates mb-1 gene transcription at the early stages of B cell differentiation. *EMBO J.* **10**, 3409-3417.
Hagman, J., Gutch, M. J., Lin, H. and Grosschedl, R. (1995). EBF contains a novel zinc coordination motif and multiple dimerization and transcriptional activation domains. *EMBO J.* **14**, 2907-2916.
Hattori, Y., Sugimura, K. and Uemura, T. (2007). Selective expression of Knot/Collier, a transcriptional regulator of the EBF/Olf-1 family, endows the Drosophila sensory system with neuronal class-specific elaborated dendritic patterns. *Genes Cells* **12**, 1011-1022.
Hatzold, J. and Conradt, B. (2008). Control of apoptosis by asymmetric cell division. *PLoS Biol.* **6**, pe84.
Hedgecock, E. M., Culotti, J. G. and Hall, D. H. (1990). The unc-5, unc-6, and unc-40 genes guide circumferential migrations of pioneer axons and mesodermal cells on the epidermis in C. elegans. *Neuron* **4**, 61-85.
Hengartner, M. O., Ellis, R. and Horvitz, R. (1992). Caenorhabditis elegans gene ced-9 protects cells from programmed cell death. *Nature* **356**, 494-499.
Hirose, T., Galvin, B. D. and Horvitz, H. R. (2010). Six and Eya promote apoptosis through direct transcriptional activation of the proapoptotic BH3-only gene egl-1 in Caenorhabditis elegans. *Proc. Natl. Acad. Sci. USA* **107**, 15479-15484.
Horvitz, H. R., Shaham, S. and Hengartner, M. O. (1994). The genetics of programmed cell death in the nematode Caenorhabditis elegans. *Cold Spring Harb. Symp. Quant. Biol.* **59**, 377-385.
Jin, K. and Xiang, M. (2011). Ebf1 deficiency causes increase of Muller cells in the retina and abnormal topographic projection at the optic chiasm. *Biochem. Biophys. Res. Commun.* **414**, 539-544.
Kieslinger, M., Folberth, S., Dobreva, G., Dorn, T., Croci, L., Erben, R., Consalez, G. G. and Grosschedl, R. (2005). EBF2 regulates osteoblast-dependent differentiation of osteoclasts. *Dev. Cell* **9**, 757-767.
Kim, K. and Li, C. (2004). Expression and regulation of an FMRFamide-related neuropeptide gene family in Caenorhabditis elegans. *J. Comp. Neurol.* **475**, 540-550.
Kim, K., Colosimo, M. E., Yeung, H. and Sengupta, P. (2005). The UNC-3 Olf/EBF protein represses alternate neuronal programs to specify chemosensory neuron identity. *Dev. Biol.* **286**, 136-148.
Kimble, J. and Hirsh, D. (1979). The postembryonic cell lineages of the hermaphrodite and male gonads in Caenorhabditis elegans. *Dev. Biol.* **70**, 396-417.
Kratsios, P., Stolfi, A., Levine, M. and Hobert, O. (2012). Coordinated regulation of cholinergic motor neuron traits through a conserved terminal selector gene. *Nat. Neurosci.* **15**, 205-214.
Latchman, D. S. (1997). Transcription factors: an overview. *Int. J. Biochem. Cell Biol.* **29**, 1305-1312.
Liao, D. (2009). Emerging roles of the EBF family of transcription factors in tumor suppression. *Mol. Cancer Res.* **7**, 1893-1901.
Liberg, D., Sigvardsson, M. and Akerblad, P. (2002). The EBF/Olf/Collier family of transcription factors: regulators of differentiation in cells originating from all three embryonal germ layers. *Mol. Cell. Biol.* **22**, 8389-8397.
Lin, H. and Grosschedl, R. (1995). Failure of B-cell differentiation in mice lacking the transcription factor EBF. *Nature* **376**, 263-267.
Liu, H., Strauss, T. J., Potts, M. B. and Cameron, S. (2006). Direct regulation of egl-1 and of programmed cell death by the Hox protein MAB-5 and by CEH-20, a C. elegans homolog of Pbx1. *Development* **133**, 641-650.
Maurer, C. W., Chiorazzi, M. and Shaham, S. (2007). Timing of the onset of a developmental cell death is controlled by transcriptional induction of the C. elegans ced-3 caspase-encoding gene. *Development* **134**, 1357-1368.
Mega, T., Lupia, M., Amodio, N., Horton, S. J., Mesuraca, M., Pelaggi, D., Agosti, V., Grieco, M., Chiarella, E., Spina, R. et al. (2011). Zinc finger protein 521 antagonizes early B-cell factor 1 and modulates the B-lymphoid differentiation of primary hematopoietic progenitors. *Cell Cycle* **10**, 2129-2139.
Nehme, R. and Conradt, B. (2008). egl-1: a key activator of apoptotic cell death in C. elegans. *Oncogene* **27** Suppl. 1, S30-S40.
Nehme, R., Grote, P., Tomasi, T., Löser, S., Holzkamp, H., Schnabel, R. and Conradt, B. (2010). Transcriptional upregulation of both egl-1 BH3-only and ced-3 caspase is required for the death of the male-specific CEM neurons. *Cell Death Differ.* **17**, 1266-1276.
Oppenheim, R. W. (1991). Cell death during development of the nervous system. *Annu. Rev. Neurosci.* **14**, 453-501.
Potts, M. B., Wang, D. P. and Cameron, S. (2009). Trithorax, Hox, and TALE-class homeodomain proteins ensure cell survival through repression of the BH3-only gene egl-1. *Dev. Biol.* **329**, 374-385.
Prasad, B. C., Ye, B., Zackhary, R., Schrader, K., Seydoux, G. and Reed, R. R. (1998). unc-3, a gene required for axonal guidance in Caenorhabditis elegans, encodes a member of the O/E family of transcription factors. *Development* **125**, 1561-1568.
Prasad, B., Karakuzu, O., Reed, R. R. and Cameron, S. (2008). unc-3-dependent repression of specific motor neuron fates in Caenorhabditis elegans. *Dev. Biol.* **323**, 207-215.
Richard, J. P., Zuryn, S., Fischer, N., Pavet, V., Vaucamps, N. and Jarriault, S. (2011). Direct in vivo cellular reprogramming involves transition through discrete, non-pluripotent steps. *Development* **138**, 1483-1492.
Sulston, J. E. and Horvitz, H. R. (1981). Abnormal cell lineages in mutants of the nematode Caenorhabditis elegans. *Dev. Biol.* **82**, 41-55.
Sulston, J. E., Schierenberg, E., White, J. G. and Thomson, J. N. (1983). The embryonic cell lineage of the nematode Caenorhabditis elegans. *Dev. Biol.* **100**, 64-119.
Thellmann, M., Hatzold, J. and Conradt, B. (2003). The Snail-like CES-1 protein of C. elegans can block the expression of the BH3-only cell-death activator gene egl-1 by antagonizing the function of bHLH proteins. *Development* **130**, 4057-4071.
Tsai, R. Y. and Reed, R. R. (1997). Cloning and functional characterization of Roaz, a zinc finger protein that interacts with O/E-1 to regulate gene expression: implications for olfactory neuronal development. *J. Neurosci.* **17**, 4159-4169.
Tsalik, E. L., Niacaris, T., Wenick, A. S., Pau, K., Avery, L. and Hobert, O. (2003). LIM homeobox gene-dependent expression of biogenic amine receptors in restricted regions of the C. elegans nervous system. *Dev. Biol.* **263**, 81-102.
Tursun, B., Cochella, L., Carrera, I. and Hobert, O. (2009). A toolkit and robust pipeline for the generation of fosmid-based reporter genes in C. elegans. *PLoS ONE* **4**, e4625.
Wang, M. M., Tsai, R. Y., Schrader, K. A. and Reed, R. R. (1993). Genes encoding components of the olfactory signal transduction cascade contain a DNA binding site that may direct neuronal expression. *Mol. Cell. Biol.* **13**, 5805-5813.
Wang, X., Yang, C., Chai, J., Shi, Y. and Xue, D. (2002). Mechanisms of AIF-mediated apoptotic DNA degradation in Caenorhabditis elegans. *Science* **298**, 1587-1592.
Wang, S. S., Lewcock, J. W., Feinstein, P., Mombaerts, P. and Reed, R. R. (2004). Genetic disruptions of O/E2 and O/E3 genes reveal involvement in olfactory receptor neuron projection. *Development* **131**, 1377-1388.
White, J. G., Southgate, E., Thomson, J. N. and Brenner, S. (1986). The structure of the nervous system of the nematode Caenorhabditis elegans. *Philos. Trans. R. Soc. Lond. B Biol. Sci.* **314**, 1-340.
Wightman, B., Baran, R. and Garriga, G. (1997). Genes that guide growth cones along the C. elegans ventral nerve cord. *Development* **124**, 2571-2580.
Yang, M., Sun, J., Sun, X., Shen, Q., Gao, Z. and Yang, C. (2009). Caenorhabditis elegans protein arginine methyltransferase PRMT-5 negatively regulates DNA damage-induced apoptosis. *PLoS Genet.* **5**, e1000514.
Yuan, J. and Horvitz, H. R. (1992). The Caenorhabditis elegans cell death gene ced-4 encodes a novel protein and is expressed during the period of extensive programmed cell death. *Development* **116**, 309-320.
Zahn, T. R., Angleson, J. K., MacMorris, M. A., Domke, E., Hutton, J. F., Schwartz, C. and Hutton, J. C. (2004). Dense core vesicle dynamics in Caenorhabditis elegans neurons and the role of kinesin UNC-104. *Traffic* **5**, 544-559.
Zandi, S., Mansson, R., Tsapogas, P., Zetterblad, J., Bryder, D. and Sigvardsson, M. (2008). EBF1 is essential for B-lineage priming and establishment of a transcription factor network in common lymphoid progenitors. *J. Immunol.* **181**, 3364-3372.
Zhao, F., McCarrick-Walmsley, R., Akerblad, P., Sigvardsson, M. and Kadesch, T. (2003). Inhibition of p300/CBP by early B-cell factor. *Mol. Cell. Biol.* **23**, 3837-3846.
Zhao, L. Y., Niu, Y., Santiago, A., Liu, J., Albert, S. H., Robertson, K. D. and Liao, D. (2006). An EBF3-mediated transcriptional program that induces cell cycle arrest and apoptosis. *Cancer Res.* **66**, 9445-9452.
Zuryn, S., Ahier, A., Portoso, M., White, E. R., Morin, M.-C., Margueron, R. and Jarriault, S. (2014). Sequential histone-modifying activities determine the robustness of transdifferentiation. *Science* **345**, 826-829.